

Article

Structure, Mechanical and Tribological Properties of MoSN/MoS₂ Multilayer Films

Yanlong Fu ^{1,2}, Tengfei He ², Wu Yang ^{1,*}, Jiao Xu ^{2,*}, Bo Mu ³, Xianjuan Pang ⁴ and Peng Wang ²

¹ College of Chemistry and Chemical Engineering, Northwest Normal University, Lanzhou 730070, China; fyanl@licp.cas.cn

² State Key Laboratory of Solid Lubrication, Lanzhou Institute of Chemical Physics, Chinese Academy of Sciences, Lanzhou 730000, China; licp603@licp.cas.cn (T.H.); pengwang@licp.cas.cn (P.W.)

³ College of Petrochemical Technology, Lanzhou University of Technology, Lanzhou 730050, China; mubo@licp.cas.cn

⁴ National United Engineering Laboratory for Advanced Bearing Tribology, Henan University of Science and Technology, Kaifeng 475001, China; xjpang2001@haust.edu.cn

* Correspondence: yangwu@nwnu.edu.cn (W.Y.); xujiao@licp.cas.cn (J.X.); Tel.: +86-931-7971989 (W.Y.); +86-931-4968091 (J.X.)

Received: 26 December 2018; Accepted: 6 February 2019; Published: 10 February 2019



Abstract: MoSN/MoS₂ multilayer films were deposited by a sputtering MoS₂ target in alternate Ar and Ar/N₂ mixed atmospheres with different nitrogen flow rates. The influence of nitrogen flow rates on the microstructure, mechanical and tribological properties of the prepared films were investigated. The multilayer film exhibited the preferred orientation of (002) plane for MoS₂ sublayers and amorphous structure for MoSN sublayers. Introducing N₂ into the source gas resulted in a much more compact structure for multilayer films due to the suppression of columnar growth of MoS₂ film. With the increase of the nitrogen flow rate, the hardness of the multilayer film firstly increased from 2.3 to 10.5 GPa as the nitrogen flow rate increased from 4 to 10 sccm and then turned downwards to 6.5 GPa at 20 sccm. MoSN/MoS₂ film deposited with an optimized microstructure exhibited low friction coefficients below 0.03 and a wear life higher than 1.8×10^5 revolutions in vacuum. Meanwhile, the optimized film showed an ultralow friction coefficient of 0.004~0.01 and wear rate of 4.7×10^{-7} mm³/N·m in an ultrahigh vacuum. Both the enhanced hardness by N-doping and sustainable formed MoS₂ tribofilm contributed to the improved tribological property of MoSN/MoS₂ multilayer film.

Keywords: multilayer film; nitrogen flow rate; film structure; ultralow friction

1. Introduction

Transition metal dichalcogenides (TMDs), typically MoS₂ and WS₂, are well known as excellent solid lubricants due to the weak van der Waals interactions between basal planes [1–5], which allows for an easy shearing along the direction parallel to the sheets and thereby, leading to low friction coefficients in vacuum and dry inert atmospheres [4]. Sputtering-deposited MoS₂ films generally exhibit porous structure, low hardness, low-bearing capacity, and high wear rate [6–10]. Some methods have been developed to date to improve the density, hardness and tribological properties of sputtered TMDs films, either by doping with other elements [5–7,10–15] or fabricating multilayered structures such as MoS₂/WS₂ [1,16–18], MoS₂/metal [19,20], MoS₂/a-C:H [2] and MoS₂/DLC multilayer films [21,22].

The incorporation of metallic elements into the MoS₂ is a common solution to improve the mechanical and tribological property of the MoS₂ films [6,10,23,24]. It has been investigated that the doped MoS₂ film with the optimum doping level of Cr or Ti showed both a low friction coefficient and wear rate even in moist atmosphere [10]. Non-metallic elements, especially nitrogen and carbon,

were also good candidates for doping the MoS₂ films. For the first time, Nossa et al. reported that the sputtered W-S-N film exhibited an amorphous structure and low friction coefficients [12–15]. Recently, Polcar et al. [25,26] further investigated the tribological property of the amorphous W-S-N films, which showed an ultralow friction coefficient of 0.003, a long sliding distance due to the high load-bearing capacity and formed well-oriented WS₂ tribolayers [26]. Moreover, Kadas et al. [27] focused on the atomic-level structure and chemical bonding arrangements in amorphous W-S-N films (37 at.% N), and further explained the mechanism of ultralow friction performance of the W-S-N films. It was believed that the continuous tribofilm formation of WS₂ in the contact region as well as the swift removal of excess nitrogen contributed to the ultra-low friction. Similarly, the N⁺ modified MoS₂ films also exhibited a dense structure and good film–substrate adherence. Compared to sputtered MoS₂ film, N⁺ implanted MoS₂ film showed a twofold increase of the wear life in vacuum while an increased friction coefficient was shown due to the loss of sulfur induced by N⁺ implantation [28]. In our previous work, the deposited Mo-S-N composite films [5] exhibited a much more compact amorphous structure by doping MoS₂ with nitrogen. However, high nitrogen content exceeding 17 at.% for the Mo-S-N film was unfavorable for the tribological performance improvement, since the formation of a non-lubricious metal nitrides phase was adverse for forming continuous tribofilm [5,27,29].

Additionally, compared to monolayer films, multilayer films [16–22] prepared by the alternate deposition of soft/hard sublayers in nanoscale modulation periods exhibited superior hardness and moderate residual stress [30–32]. Several explanations have been proposed to explain the hardening of multilayer film, such as dislocation blocking by layer interfaces [33,34], Hall-Petch strengthening [35], and strain effects at layer interfaces [36]. Meanwhile, the mechanical and tribological properties of multilayer films are generally related with the composition [16], grain size [18] and inter-diffusion state of the layered interface [35]. With the crystallite size and modulation period among nanometer dimensions, the interface was postulated to act as a barrier against dislocation motion [5] and resulted in an improved hardness.

In this study, a novel strategy by sputtering the MoS₂ target in alternate atmospheres of argon and argon/nitrogen mixed gases was used for the preparation of the MoSN/MoS₂ multilayer films through N doping or not, periodically. By controlling the flow rate of nitrogen during film deposition, MoSN/MoS₂ films with different nitrogen contents were prepared. The influence of N doping on the microstructure, hardness and tribological properties of the prepared MoSN/MoS₂ film was investigated in detail. Cooperative optimization of film hardness and vacuum lubricating performance were achieved for the MoSN/MoS₂ film deposited at an N₂ flow rate of 6 sccm, whereas more N₂ beyond the optimized value would degrade the film lubricating performance. The optimized film exhibited an ultralow friction coefficient and wear rate in ultrahigh vacuum condition, and the lubrication mechanism was investigated via structure analysis of the transfer film.

2. Materials and Methods

2.1. Deposition of MoSN/MoS₂ Multilayer Films

The MoSN/MoS₂ multilayer films were deposited on p-type Si (100) substrates by radio frequency magnetron sputtering of the MoS₂ target in pure argon and Ar/N₂ mixed atmosphere alternately. Details of the deposition system were reported elsewhere [7]. Prior to deposition, the Si wafers were ultrasonically cleaned in alcohol for 20 min and then placed on a sample disc under the sputtered target at a distance of 80 mm. When the vacuum chamber was pumped to a base pressure superior to 1.3×10^{-3} Pa, the substrates were etched by Ar⁺ at a pulse bias voltage of –500 V with 30% duty cycle for 20 min. Before the MoSN/MoS₂ film deposition, a Ti interlayer with a thickness of about 200 nm was firstly deposited. Then the MoSN sublayer and MoS₂ sublayer were alternately deposited with a modulation ratio of 1:1 and modulation period of 30 nm by switching on and off the inlet valve of nitrogen gas. The MoSN/MoS₂ multilayer films were deposited by r.f. sputtering the MoS₂ target with a power of 275 W under a working pressure of 0.75 Pa controlled by a constant Ar flow rate of 40 sccm

and different N₂ flow rates of 4, 6, 10, and 20 sccm, respectively. During the film deposition, the rotating speed of the sample holder was set as 1.5 r/min and the chamber temperature was controlled at 150 °C. The prepared MoSN/MoS₂ multilayer films were denoted as N4, N6, N10 and N20 films corresponding to the N₂ flow rates of 4, 6, 10, and 20 sccm, respectively. An MoSN monolayer was also deposited with a fixed nitrogen flow rate of 6 sccm while other parameters were the same as that for the MoSN/MoS₂ deposition. The total thickness of each coating was controlled to about 1.5 μm.

2.2. Structure and Chemical Characterization of MoSN/MoS₂ Multilayer Films

The surface and cross-sectional microstructures of pure MoS₂ film and MoSN/MoS₂ multilayer films were investigated by field-emission scanning electron microscopy (FESEM, JSM-6701F, JEOL, Tokyo, Japan) and transmission electron microscope (TEM, TECNAI G2 S-TWIN F20, FEI, Hillsboro, OH, USA); accelerating voltage 200 kV). The ultrathin slices for cross-section HRTEM observation were prepared by the Focused Ion Beam (FIB) technique. The crystal structure of deposited films was characterized by grazing incidence X-ray diffraction (GIXRD, Rigaku RINT2400, Kyoto, Japan) operating with Cu Kα radiation (40 kV, 150 mA, λ = 1.54056 Å) at 2° incident angle, and the diffraction angle started from 10° to 90°. The Raman spectra were measured using a Horiba LabRam HR800 spectrometer (Horiba, Tokyo, Japan) with a 532 nm wavelength excitation. The hardness and elastic modulus of the deposited films were determined by a Nano-indenter DCM nano-mechanical system (MTS, Eden Prairie, MN, USA) with a Berkovich diamond tip. The maximum indentation depth was set to 100 nm (less than 10% of film thickness) in order to minimize the effects of the substrate [37,38]. Five repeated indentations were made in a random area for each sample. The chemical composition of the deposited films was investigated by using Energy dispersive spectroscopy (EDS, JSM-5601LV, JEOL). The sample standards of C, N, O, S and Mo for element concentration calculation are C, BN, SiO₂, FeS₂, and Mo, respectively. Peak intensities from EDS spectra were calculated by least-squares fitting of sample spectra using peaks that have been previously measured and stored as references for rapid assessment of tested samples [39]. The conversion of measured X-ray intensities to element concentrations was conducted via eXtended Pouchou and Pichoir correction [40], which is a built-in part of testing software running in data report exporting. The quantitative results of XPP correction are better than other methods such as ZAF and PRZ [$\phi(\rho z)$] when heavy and light elements exist in the same sample.

2.3. Ball-on-Disk Tribotests in Vacuum Environment

The tribological properties of the prepared films were tested on a standard ball-on-disk tribometer (WTM-2E, Licp, Lanzhou, China), using GCr15 steel balls with diameters of 3 mm as sliding counterparts. The sliding tests were executed in a high vacuum of 1.3×10^{-3} Pa under a normal load of 3 N corresponding to a Hertz contact pressure of 1.5 GPa. The rotating speed was set as 1000 r/min (i.e., 0.314 m/s in linear speed), and the maximum sliding distance was 1.8×10^5 revolutions in 3 h. As the friction coefficient exceeded 0.1, the test would be stopped automatically. After friction tests, the morphologies of wear tracks were measured using Micro-XAM-3D non-contact surface profilometry (AD Corporation, Cambridge, MA, USA), and the film wear rates were calculated via the formula $K=V/(N \cdot S)$, where V is the wear volume (mm³), N is the normal load applied on the ball counterpart (N), and S is the sliding distance (m). The optical micrographs of wear scars on the ball counterpart were obtained by an optical microscope (STM6, Olympus, Tokyo, Japan).

3. Results and Discussion

3.1. Structure Characterizations of MoSN/MoS₂ Multilayer Films

The surface cross-sectional SEM images of MoSN/MoS₂ multilayer films are shown in Figure 1. Compared to the porous and columnar structure of pure MoS₂ film, the MoSN/MoS₂ multilayer films showed a dense structure particularly for the film deposited with the nitrogen gas flow rate of 6 sccm,

and the microcracks along the direction of film growth are significantly blocked. Taking N6-film for example, closer observations by cross-sectional HRTEM are shown in Figure 2, in which the bright gray and dark layers corresponded to MoS₂ and MoSN sublayers, respectively. It revealed a well-defined multilayer structure throughout the film thickness with a modulation period of about 30 nm as determined from Figure 2a,b. The MoS₂ sublayers with thicknesses of about 14.7 nm were mainly composed of cross-linked MoS₂ molecular layers, and the MoSN sublayers with thicknesses of about 15.4 nm showed an amorphous structure. The inset SAED pattern of Figure 2b1 shows the diffraction rings of MoS₂ phase, which indicates a dominant of the preferred (002) plane of the MoS₂ sublayer. With the nitrogen doped into the MoS₂, the growth of the MoS₂ crystal would be interrupted for the MoSN sublayer and the MoSN sublayers exhibited amorphous structure, which was mainly due to the formation of the Mo-N bonding by partly replacing the sulfur atom with nitrogen in the lattice of MoS₂ phase [5,26].

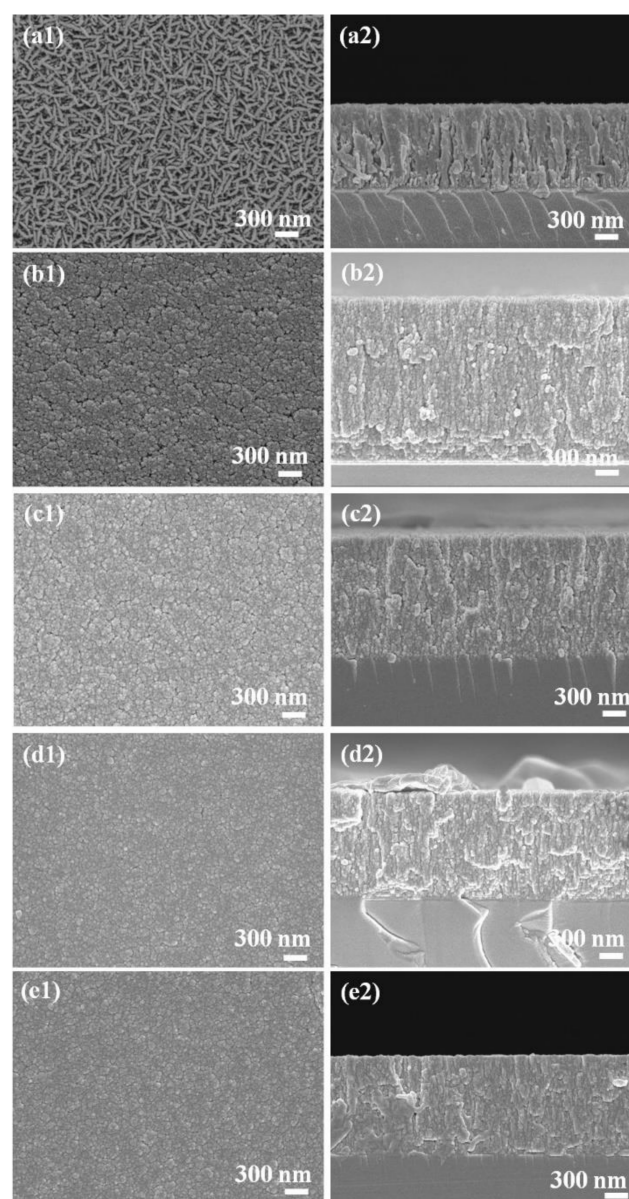


Figure 1. The top-view and cross-sectional SEM images of pure MoS₂ film and MoSN/MoS₂ multilayer films deposited with different nitrogen flow rates. (a1, a2) Pure MoS₂ film; (b1, b2) N4 film; (c1, c2) N6 film; (d1, d2) N10 film; and (e1, e2) N20 film.

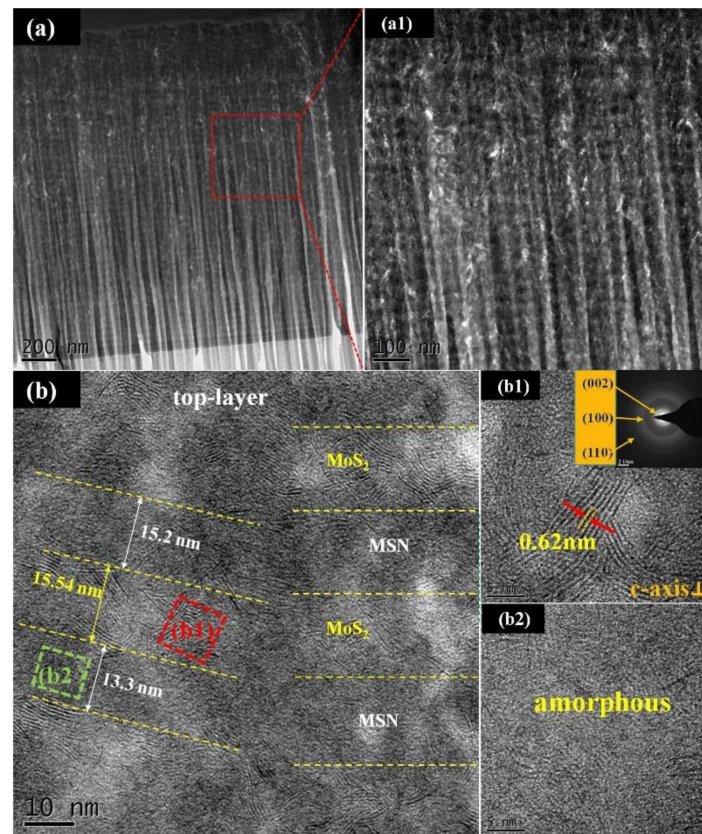


Figure 2. The cross-sectional HRTEM images of MoSN/MoS₂ multilayer film N6. (a) An overview of the FIB-prepared slice for HRTEM experiments, and (a1) the magnified image of the selected region in (a); (b) the high-resolution image of the multilayer structure with closer observations of (b1) MoS₂ and (b2) MoSN sublayers.

The Raman spectra of pure MoS₂ film and MoSN/MoS₂ multilayer films are shown in Figure 3a. Moreover, the spectrum of the MoSN monolayer deposited at a nitrogen flow rate of 6 sccm is also plotted. In general, for pure MoS₂ film, two modes of first-order Raman activity showed well-defined peaks at 383 and 409 cm⁻¹. The 383 cm⁻¹ (E_{2g}^1) is attributed to the motion of Mo+S atoms in x - y layered plane, and the 409 cm⁻¹ (A_{1g}) is attributed to the motion of S atoms along the z axis [7]. Compared to the pure MoS₂ film, the two spectral feature peaks of the MoSN monolayer and MoSN/MoS₂ multilayer films dramatically receded, and no obvious difference can be found in the MoSN/MoS₂ multilayer films deposited with different nitrogen flow rates. It is suggested that the introduction of the N atom in MoSN sublayers inhibited the crystallinity of MoS₂ both in MoS₂ and MoSN sublayers. Based on this, the crystallinity of deposited films was further characterized by GIXRD, and the results are shown in Figure 3b. Compared to the pure MoS₂ film with (002) peak at $2\theta \approx 13^\circ$ and (100) peak at $2\theta \approx 33^\circ$, the peaks of multilayer films became broad and the peak intensity reduced notably due to the fact that the deposited MoS₂ sublayer exhibited a nanocrystalline structure while the MoSN sublayer showed a nearly amorphous structure as confirmed from the HRTEM images in Figure 2.

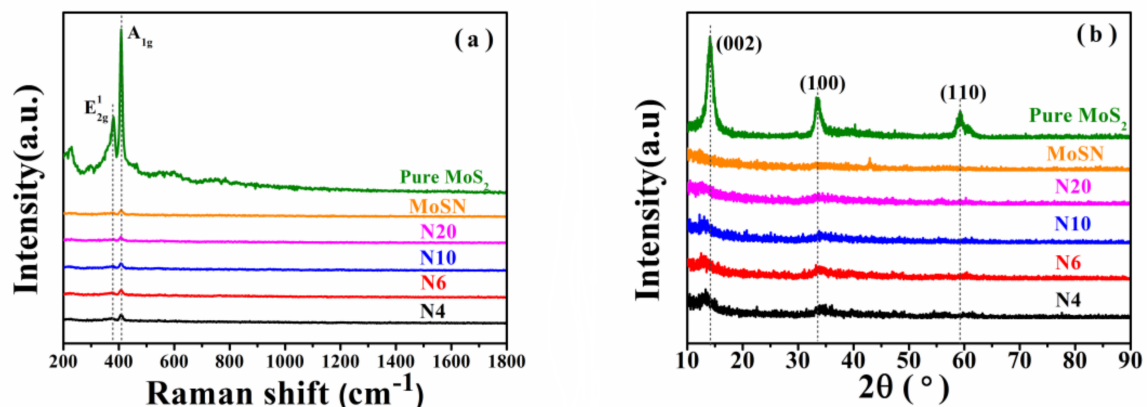


Figure 3. The structure characterization and XRD patterns of pure MoS₂ film, MoSN monolayer and MoSN/MoS₂ multilayer films deposited with different nitrogen flow rates. (a) Raman spectra and (b) glancing angle XRD patterns of studied films.

Putting aside the alternate composition of MoS₂ and MoSN sublayers, the mean chemical composition characterization of multilayer films characterized by EDS is listed in Table 1 as follows. It is noted that here the content of carbon cannot be excluded due to the usage of a beryllium window in the EDS testing system [7] and the carbon tapes on the sample holder. As a result, an offset carbon content around 25 ± 3 at.% was observed as a background in pure MoS₂ film and was not manually subtracted from the carbon contents of other multilayer films. Clearly it is seen that the S/M ratio of pure MoS₂ film is the highest one at 1.86, and the S/M ratio of the MoSN monolayer deposited with 6 sccm N₂ is slightly lower than that of the N6 multilayer film. Moreover, a clear tendency is seen that by increasing the nitrogen flow rates for 4 to 20 sccm, the S/M ratio in multilayer films gradually decreases from 1.58 to 1.03. A similar tendency has been reported in the literature for sputter deposited MoSN [5] and WSN films [26].

Table 1. The chemical composition of pure MoS₂ film, MoSN monolayer and MoS₂/MoSN multilayer films characterization by EDS.

Samples	Chemical Composition (at.%)			
	N	C	O	S/Mo
pure MoS ₂	0	25.2	2.5	1.86
MoSN monolayer	5.2	23.7	4.1	1.31
N4	3.6	25.8	3.6	1.58
N6	4.8	23.4	5.2	1.42
N10	7.9	23.7	2.8	1.28
N20	10.3	27.3	3.5	1.03

3.2. Mechanical Properties of MoSN/MoS₂ Multilayer Films

The mechanical properties of sputtered MoS₂ film, MoSN monolayer and MoSN/MoS₂ multilayer films are presented in Figure 4. It can be seen that the hardness of multilayer films firstly rise with the increase of the N₂ flow rate to 10.3 GPa at 10 sccm, which is dozens of times higher than that of 0.15 GPa for pure MoS₂ film, and then descends to 6.5 GPa at 20 sccm. The inset curves displayed the corresponding load-displacement curves, and the elastic recovery ratios of multilayer films were consistent with the varying tendency of film hardness, showing the maximum elastic recovery ratio to 41.4% at 10 sccm. The MoSN monolayer showed the highest hardness and elastic modulus of 11.6 and 134.6 GPa, respectively, and its elastic recovery ratio was similar to the N10 film. In contrast to the pure sputtered MoS₂ film, the optimization of N₂ flow rate induces a high resistance of plastic deformation and load-bearing capacity for composite and multilayer films. In fact, the increased hardness of

MoS₂/MoSN multilayer films is closely related to the high hardness of MoSN sublayers and the interface strengthening effects (e.g., interfacial mixing, interface density and interfacial roughness) of the multilayer structure. As it is known, the multilayer interface may be postulated to act as a barrier against the dislocation motion and/or crack deflection. Moreover, the reduced crystallite size is also a key factor at the origin of increased yield strength and hardness enhancement, such like in a large variety of molybdenum disulfide [17,19,20] and nitride-based multilayer films [30,32,41–44]. Thus, the interfaces of MoSN hard sublayers and MoS₂ soft sublayers may preferably hinder the dislocation slip to prevent plastic deformation, so as to improve the film hardness.

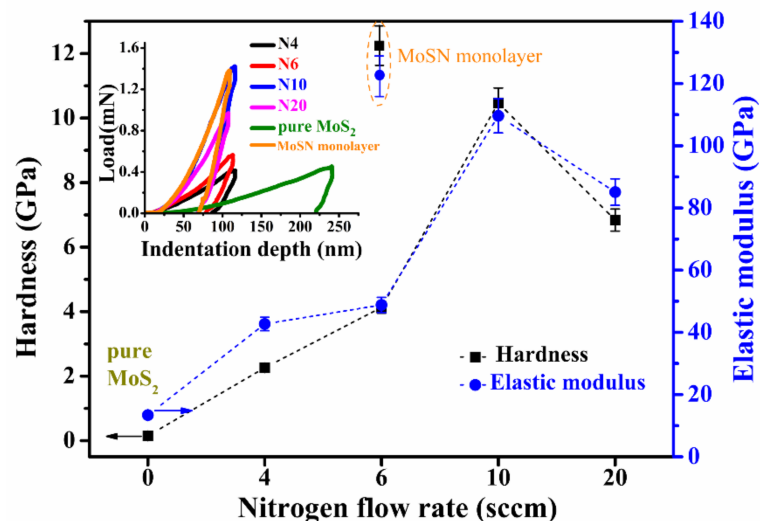


Figure 4. Hardness and elastic modulus of pure MoS₂ film, MoSN monolayer and MoSN/MoS₂ multilayer films with different nitrogen flow rates. The corresponding load-displacement curves are inserted.

3.3. Tribological Properties of MoSN/MoS₂ Multilayer Films

The friction coefficients and wear rates of MoSN/MoS₂ multilayer films prepared in different nitrogen flow rates were investigated using a standard ball-on-disc tribometer in a high vacuum environment, and the results are displayed in Figure 5. As shown in Figure 5a, the mean friction coefficients of multilayer films generally maintained a steady state of 0.02–0.04, while the film wear lives were longer than 1.8×10^5 revolutions for films deposited with nitrogen flow rates of 4 and 6 sccm and then dramatically decreased in the case of 10 and 20 sccm. Further, tribotests lasting for 2.0×10^4 revolutions were conducted to evaluate the wear rates in steady state friction for all the films. The two-dimensional profiles of wear tracks and calculated wear rates for the films are shown in Figure 5b. It can be seen that the wear rates of the MoSN monolayer and MoSN/MoS₂ multilayer films were generally below the level of 1.0×10^{-6} mm³/N·m, which was much lower than that of the pure MoS₂ film. However, it was shown that the pure MoS₂ film exhibited wear lives close to 4.0×10^4 revolutions, which was comparable to that for the MoSN monolayer and N20 film, although the wear rate of the pure MoS₂ film was much higher than the latter two films. One reasonable explanation is that the anti-wear property of tribofilm derived from pure MoS₂ film was more reliable than that of the latter two films, especially in the friction state after 2.0×10^4 revolutions. In the case of pure MoS₂ film, the film was quickly worn out during the first 2.0×10^4 revolutions, yet the resulting tribofilm may have sustained the low-friction state during the following 2.0×10^4 revolutions. By contrast, the MoSN monolayer and N20 film exhibited low friction and wear in the first 2.0×10^4 revolutions, yet the tribofilms were quickly damaged afterwards. Such a sudden failure of N-incorporated MoS₂-based films was also found particularly with high N-doped concentrations [5]. Although the film hardness can be improved considerably by increasing the N concentration, the hexagonal layer structure of

MoS₂ would be severely disturbed due to the loss of S atoms, so that the sustainable formation of MoS₂ tribofilm may be impeded [5,27,45]. The optical micrographs of wear scars, as shown in Figure 6, also suggested that the counterfaces sliding against N4 and N6 films were fully covered by tribofilm in contrast to the N10 and N20 films. While, for the film with low nitrogen content, the N6 film exhibited a lower wear rate compared to the N4 film, which was mainly due to the higher hardness of the N6 film. Hence, it can be deduced that the optimum nitrogen content in MoSN sublayers is beneficial for improving the film harness and well-formed tribofilm, which was favorable to maintain a low wear rate and long wear life of MoSN/MoS₂ multilayer film.

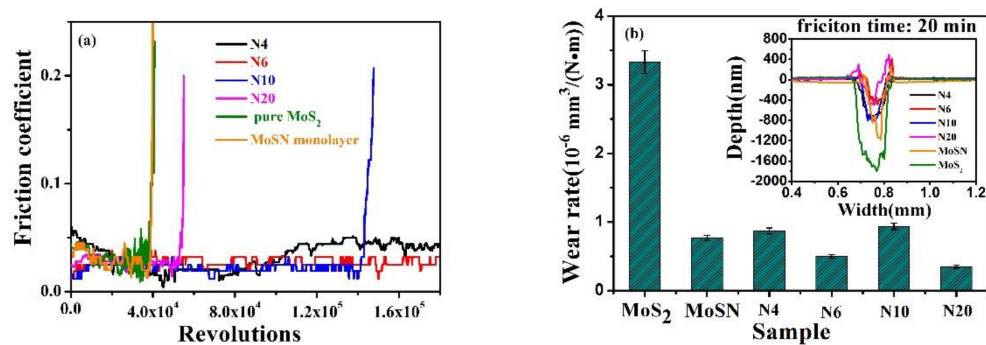


Figure 5. The friction coefficient curves of pure MoS₂ film, MoSN monolayer and MoSN/MoS₂ multilayer films in a high vacuum (1.3×10^{-3} Pa) environment. (a) The friction coefficient curves and (b) the film wear rates in the first 2.0×10^4 revolutions; the inset shows the two-dimensional profiles of the wear track.

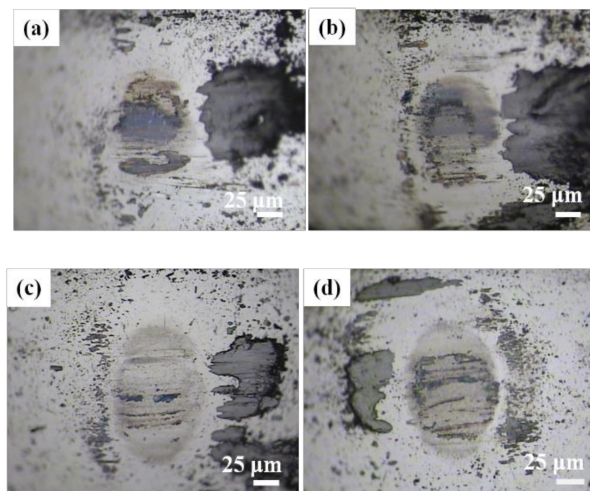


Figure 6. The optical micrographs of worn balls sliding against the MoSN/MoS₂ multilayer films of (a) N4, (b) N6, (c) N10, and (d) N20 for 2.0×10^4 revolutions.

Later, the anti-wear properties of N6 and N10 films were further investigated under an ultrahigh vacuum condition ($<10^{-5}$ Pa) close to the space environment, and the results are shown in Figure 7. In this test, N6 and N10 films showed ultralow friction coefficients below 0.01 after certain circles of a running-in period, and the frictionless state kept longer than 6.0×10^4 revolutions. Specifically, the friction coefficients firstly reduced to 0.01 at 9.6×10^3 revolutions, and further gradually decreased to 0.004 at 2.4×10^4 revolutions and then exhibited an ultra-low friction coefficient for 85 min before rising back to 0.03 after 1.09×10^5 revolutions for the N6 film. By comparison, the N10 film exhibited ultralow friction coefficients around 0.008 during 6.8×10^4 – 1.3×10^5 revolutions. Figure 8 shows the wear scars and tracks formed in ultrahigh vacuum condition after 1.8×10^5 revolutions for the two films. Clearly, the width and depth of the wear track for the N10 film were much larger than that for

the N6 film, and the wear rates of the N6 and N10 films were 4.7×10^{-7} and 7.0×10^{-7} $\text{mm}^3/\text{N}\cdot\text{m}$, respectively, which was comparable to the results observed in the high vacuum condition (see in Figure 5b). However, it was noticed that wear tracks exhibited 1.73 and 1.48 μm in depth for the N6 and N10 films, respectively, which were approximate to the film thickness. This suggested that even when the films were nearly worn out, the friction-induced tribofilms could still play an effective role in contributing to the low friction coefficient below 0.04.

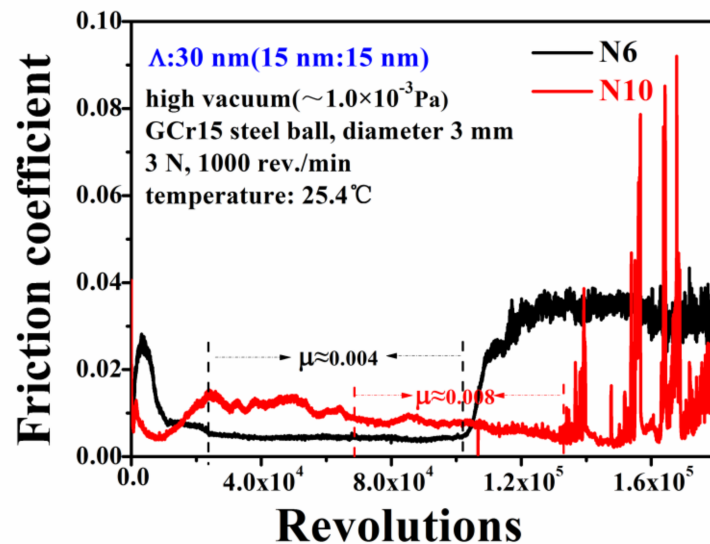


Figure 7. The friction coefficient curves of MoSN/MoS₂ multilayer films N6 and N10 tested in an ultrahigh vacuum for 1.8×10^5 sliding revolutions.

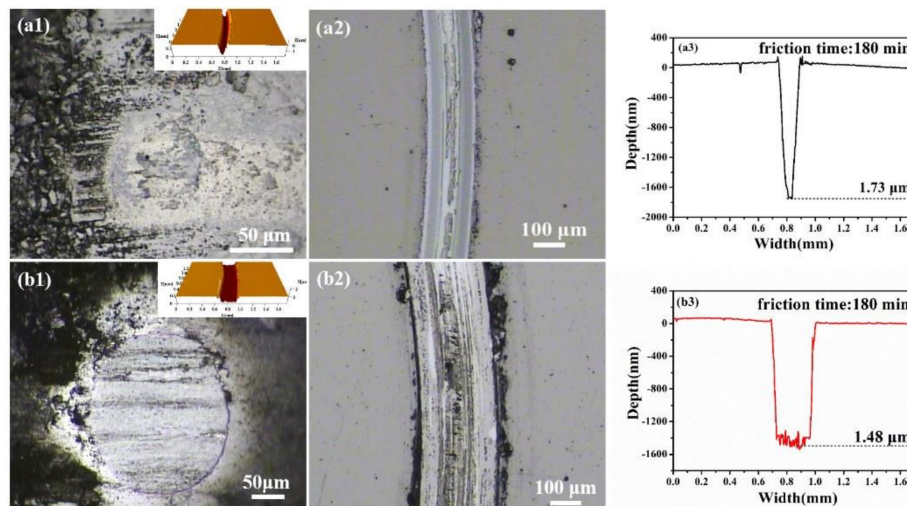


Figure 8. The optical micrographs of balls scars and wear tracks when steel balls slid against (a1,a2,a3) N6 film and (b1,b2,b3) N10 film in an ultrahigh vacuum for 1.8×10^5 revolutions. The three-dimensional surface images of wear tracks are inserted in (a1,b1), and (a3,b3) displays the corresponding two-dimensional profiles.

To confirm the tribofilm-based lubricant mechanism of the two tested films in the ultrahigh vacuum, the wear debris derived from N6 film was characterized by Raman spectroscopy, and the results are shown in Figure 9. Compared to the as-deposited film, the debris showed enhanced MoS₂ peak intensity with reduced band width, which suggested a long range re-ordering of MoS₂ phases into a lamellar structure. The same results have also been reported in the previous work

of MoSN [5], MoSC [7], MoSCN films [46] and other TMDs composite films [26,27]. According to Gustavsson et al. [26], the friction coefficient of amorphous W-S-N films was lower than 0.003 in dry nitrogen, which was attributed to the formation of WS₂ tribofilms on of the surface of the wear tracks and counterpart. Isaeva et al. [27] suggested that the ultralow friction of amorphous W-S-N films were due to a dense and stable surface, the easy access to W and S for the continuous formation of WS₂ in the contact region, the absence of high-friction and high-wear secondary phases, and the release of a nitrogen atom in molecular form. From the same point of view, Donnet et al. [4] presented that the super-low friction coefficients of MoS₂-based coatings in an ultrahigh vacuum (UHV: 10⁻⁸ Pa) and dry nitrogen conditions were attributed to the formed tribofilm with a particular combination of crystallographic orientation and the absence of contaminants, leading to a significant decrease in the interfacial shear strength [4]. In this study, the interface strengthening effects contributed to the improved mechanical strength of MoSN/MoS₂ multilayer films. In addition, the formation of a well-oriented tribofilm for the MoSN/MoS₂ multilayer film with optimized nitrogen content resulted in low friction behavior in the vacuum environment.

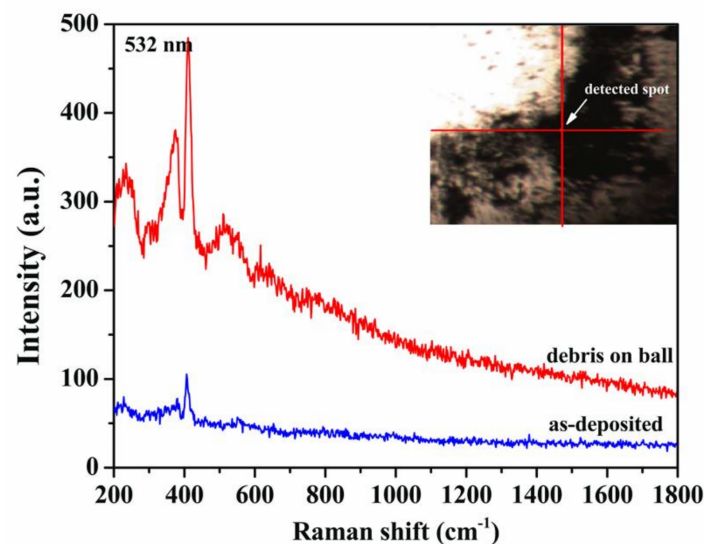


Figure 9. Raman spectra of wear debris derived from N6 films after sliding 1.8×10^5 revolutions in an ultrahigh vacuum.

4. Conclusions

In summary, by alternating the source gas of Ar or mixed Ar and N₂ during the sputtering of the MoS₂ target, MoSN/MoS₂ multilayer films were deposited. The effect of the nitrogen flow rates on the microstructures and tribological properties of the deposited MoSN/MoS₂ multilayer films was investigated. The results obtained are summarized as follows:

- By alternately depositing the MoSN and MoS₂ sublayers, the prepared MoSN/MoS₂ multilayer film exhibited a compact structure due to the suppression of the columnar growth of the sputtered MoS₂. The MoS₂ sublayers showed a nanocrystalline structure with a preferred orientation of an (002) plane while the MoSN sublayers exhibited an amorphous structure.
- The hardness of the MoSN/MoS₂ multilayer film showed a great increase compared to the MoS₂ and increased from 2.3 to 10.5 GPa as the nitrogen flow rate increased from 4 to 10 sccm. The MoSN/MoS₂ multilayer films deposited with nitrogen flow rates of 4 and 6 sccm exhibited low friction coefficients below 0.03 and wear lives higher than 1.8×10^5 revolutions in a high vacuum condition, which is much longer than that of pure MoS₂ or MoSN film. The improved wear life for the MoSN/MoS₂ multilayer with low nitrogen content was mainly attributed to the lower wear rate, which resulted from the enhanced hardness as well as the sustainably formed MoS₂ tribofilms.

- The MoSN/MoS₂ multilayer film deposited with a nitrogen flow rate of 6 sccm exhibited ultra-low friction coefficients of 0.004–0.01 and a wear rate of 4.7×10^{-7} mm³/N·m in an ultrahigh vacuum condition. The ultralow friction coefficient for the MoSN/MoS₂ multilayer film was mainly due to the formation of the MoS₂ tribofilm with a long-range ordered lamellar structure on the sliding interface.

Author Contributions: Conceptualization, W.Y. and J.X.; Methodology, Y.F. and T.H.; Formal Analysis, Y.F., T.H., B.M. and X.P.; Resources, P.W.; Writing—Original Draft Preparation, Y.F.; Writing—Review & Editing, W.Y. and J.X.

Funding: This research was funded by the National Natural Science Foundation of China (Nos. 51705503, 11475236, and U1404504).

Acknowledgments: The authors would like to thank Professor Ming Hu for excellent technical support and Desheng Wang for critically reviewing the manuscript.

Conflicts of Interest: The authors declare no conflict of interest.

References

1. Zhu, L.-N.; Wang, C.-B.; Wang, H.-D.; Xu, B.-S.; Zhuang, D.-M.; Liu, J.-J.; Li, G.-L. Microstructure and tribological properties of WS₂/MoS₂ multilayer films. *Appl. Surf. Sci.* **2012**, *258*, 1944–1948.
2. Wu, Y.; Li, H.; Ji, L.; Ye, Y.; Chen, J.; Zhou, H. A long-lifetime MoS₂/a-C:H nanoscale multilayer film with extremely low internal stress. *Surf. Coat. Tech.* **2013**, *236*, 438–443. [[CrossRef](#)]
3. Kim, S.S.; Ahn, C.W.; Kim, T.H. Tribological characteristics of magnetron sputtered MoS₂ films in various atmospheric conditions. *KSME Int. J.* **2002**, *16*, 1065–1071. [[CrossRef](#)]
4. Donnet, C.; Martin, J.M.; Le Mogne, T.; Belin, M. Super-low friction of MoS₂ coatings in various environments. *Tribol. Int.* **1996**, *29*, 123–128. [[CrossRef](#)]
5. Zhang, X.; Qiao, L.; Chai, L.; Xu, J.; Shi, L.; Wang, P. Structural, mechanical and tribological properties of Mo–S–N solid lubricant films. *Surf. Coat. Tech.* **2016**, *296*, 185–191. [[CrossRef](#)]
6. Xu, S.; Gao, X.; Hu, M.; Wang, D.; Jiang, D.; Sun, J.; Zhou, F.; Weng, L.; Liu, W. Microstructure evolution and enhanced tribological properties of Cu-doped WS₂ films. *Tribol. Lett.* **2014**, *55*, 1–13. [[CrossRef](#)]
7. Xu, J.; Chai, L.; Qiao, L.; He, T.; Wang, P. Influence of C dopant on the structure mechanical and tribological properties of r.f.-sputtered MoS₂/a-C composite. *Appl. Surf. Sci.* **2016**, *364*, 249–256. [[CrossRef](#)]
8. Fleischauer, P.D.; Lince, J.R. A comparison of oxidation and oxygen substitution in MoS₂ solid film lubricants. *Tribol. Int.* **1999**, *32*, 627–636. [[CrossRef](#)]
9. Khare, H.S.; Burris, D.L. Surface and subsurface contributions of oxidation and moisture to room temperature friction of molybdenum disulfide. *Tribol. Lett.* **2014**, *53*, 329–336. [[CrossRef](#)]
10. Ding, X.Z.; Zeng, X.T.; He, X.Y.; Chen, Z. Tribological properties of Cr- and Ti-doped MoS₂ composite coatings under different humidity atmosphere. *Surf. Coat. Tech.* **2010**, *205*, 224–231. [[CrossRef](#)]
11. Gu, L.; Ke, P.; Zou, Y.; Li, X.; Wang, A. Amorphous self-lubricant MoS₂-C sputtered coating with high hardness. *Appl. Surf. Sci.* **2015**, *33*, 166–171. [[CrossRef](#)]
12. Nossa, A.; Cavaleiro, A. Chemical and physical characterization of C(N)-doped W–S sputtered films. *J. Mater. Res.* **2004**, *19*, 2356–2365. [[CrossRef](#)]
13. Nossa, A.; Cavaleiro, A. Behaviour of nanocomposite coatings of WSN/C system under pin-on-disk testing. *Mater. Sci. Forum.* **2004**, *455*, 515–519. [[CrossRef](#)]
14. Nossa, A.; Cavaleiro, A. Tribological behaviour of N (C)-alloyed W–S films. *Tribol. Lett.* **2007**, *28*, 59–70. [[CrossRef](#)]
15. Nossa, A.; Cavaleiro, A. Mechanical behaviour of W–S–N and W–S–C sputtered coatings deposited with a Ti interlayer. *Surf. Coat. Tech.* **2003**, *163*, 552–560. [[CrossRef](#)]
16. Watanabe, S.; Noshiro, J.; Miyake, S. Tribological characteristics of WS₂/MoS₂ solid lubricating multilayer films. *Surf. Coat. Tech.* **2004**, *183*, 347–351. [[CrossRef](#)]
17. Watanabe, S.; Noshiro, J.; Miyake, S. Friction properties of WS₂/MoS₂ multilayer films under vacuum environment. *Surf. Coat. Tech.* **2004**, *188*, 644–648. [[CrossRef](#)]
18. Miyake, S.; Sekine, Y.; Noshiro, J.; Watanabe, S. Low-friction and long-life solid lubricant films structured of nanoperiod tungsten disulfide and molybdenum disulfide multilayer. *Jap. J. Appl. Phys.* **2004**, *43*, 4338. [[CrossRef](#)]

19. Mikhailov, S.; Savan, A.; Pflüger, E.; Knoblauch, L.; Hauert, R.; Simmonds, M.; Van Swygenhoven, H. Morphology and tribological properties of metal (oxide)–MoS₂ nanostructured multilayer coatings. *Surf. Coat. Tech.* **1998**, *105*, 175–183. [[CrossRef](#)]
20. Simmonds, M.C.; Savan, A.; Van Swygenhoven, H.; Pflüger, E.; Mikhailov, S. Structural, morphological, chemical and tribological investigations of sputter deposited MoS_x/metal multilayer coatings. *Surf. Coat. Tech.* **1998**, *108*, 340–344. [[CrossRef](#)]
21. Zhao, X.; Lu, Z.; Wu, G.; Zhang, G.; Wang, L.; Xue, Q. Preparation and properties of DLC/MoS₂ multilayer coatings for high humidity tribology. *Mater. Res. Exp.* **2016**, *3*, 066401. [[CrossRef](#)]
22. Wang, Y.; Chang, C.; Ho, W. Microstructure analysis of MoS₂ deposited on diamond-like carbon films for wear improvement. *Surf. Coat. Tech.* **1999**, *111*, 123–127. [[CrossRef](#)]
23. Sun, G.; Bhowmick, S.; Alpas, A.T. Effects of atmosphere and temperature on the tribological behavior of the Ti containing MoS₂ coatings against aluminum. *Tribol. Lett.* **2017**, *65*, 158. [[CrossRef](#)]
24. Zhou, H.; Zheng, J.; Wen, Q.-P.; Wan, Z.-H.; Sang, R.-P. The effect of Ti content on the structural and mechanical properties of MoS₂-Ti composite coatings deposited by unbalanced magnetron sputtering system. *Phys. Procedia.* **2011**, *18*, 234–239.
25. Mutafov, P.; Evaristo, M.; Cavaleiro, A.; Polcar, T. Structure, mechanical and tribological properties of self-lubricant W–S–N coatings. *Surf. Coat. Tech.* **2015**, *261*, 7–14. [[CrossRef](#)]
26. Gustavsson, F.; Jacobson, S.; Cavaleiro, A.; Polcar, T. Ultra-low friction W–S–N solid lubricant coating. *Surf. Coat. Tech.* **2013**, *232*, 541–548. [[CrossRef](#)]
27. Isaeva, L.; Sundberg, J.; Mukherjee, S.; Pelliccione, C.J.; Lindblad, A.; Segre, C.U.; Jansson, U.; Sarma, D.D.; Eriksson, O.; Kádas, K. Amorphous W–S–N thin films: The atomic structure behind ultra-low friction. *Acta Mater.* **2015**, *82*, 84–93. [[CrossRef](#)]
28. Liu, H.; Zhang, X. Improved tribological properties of sputtered MoS₂ films through N⁺ implantation. *Thin Solid Films* **1994**, *240*, 97–100. [[CrossRef](#)]
29. Sundberg, J.; Nyberg, H.; Särhammar, E.; Nyberg, T.; Jacobson, S.; Jansson, U. Influence of composition, structure and testing atmosphere on the tribological performance of W–S–N coatings. *Surf. Coat. Tech.* **2014**, *258*, 86–94. [[CrossRef](#)]
30. Abadias, G.; Miche, A.; Tromas, C.; Jaouen, C.; Dub, S.N. Stress Interfacial effects and mechanical properties of nanoscale multilayered coatings. *Surf. Coat. Tech.* **2007**, *202*, 844–853. [[CrossRef](#)]
31. Yashar, P.C.; Sproul, W.D. Nanometer scale multilayered hard coatings. *Vacuum* **1999**, *55*, 179–190. [[CrossRef](#)]
32. Beliardouh, N.E.; Bouzid, K.; Nouveau, C.; Tlili, B.; Walock, M.J. Tribological and electrochemical performances of Cr/CrN and Cr/CrN/CrAlN multilayer coatings deposited by RF magnetron sputtering. *Tribol. Int.* **2015**, *82*, 443–452. [[CrossRef](#)]
33. Koehler, J.S. Attempt to design a strong solid. *Phys. Rev. B* **1970**, *2*, 547. [[CrossRef](#)]
34. Chu, X.; Barnett, S.A. Model of superlattice yield stress and hardness enhancements. *J. Appl. Phys.* **1995**, *77*, 4403–4411. [[CrossRef](#)]
35. Anderson, P.M.; Li, C. Hall-Petch relations for multilayered materials. *Nanostructure Mater.* **1995**, *5*, 349–362. [[CrossRef](#)]
36. Kato, M.; Mori, T.; Schwartz, L.H. Hardening by spinodal modulated structure. *Acta Met.* **1980**, *28*, 285–290. [[CrossRef](#)]
37. Oliver, W.C.; Pharr, G.M. An improved technique for determining hardness and elastic modulus using load and displacement sensing indentation experiments. *J. Mater. Res.* **1992**, *7*, 1564–1583. [[CrossRef](#)]
38. Oliver, W.C.; Pharr, G.M. Measurement of hardness and elastic modulus by instrumented indentation: Advances in understanding and refinements to methodology. *J. Mater. Res.* **2004**, *19*, 3–20. [[CrossRef](#)]
39. Pouchou, J.L. Standardless X-ray analysis of bulk specimens. *Mikrochim Acta* **1994**, *114–115*, 33–52. [[CrossRef](#)]
40. Pouchou, J.L.; Pichoir, F.; Boivin, D. Further improvements in quantitation procedures for X-ray microanalysis. In Proceedings of the XII International Symposium on X-ray Optics and Microanalysis, Cracow, Poland, 1990; pp. 52–59.
41. Hopf, C.; Jacob, W.; Keudell, A.V. Ion-induced surface activation, chemical sputtering, and hydrogen release during plasma-assisted hydrocarbon film growth. *J. Appl. Phys.* **2005**, *094904*, 97. [[CrossRef](#)]
42. Chu, X.; Barnett, S.A.; Wong, M.S.; Sproul, W.D. Reactive unbalanced magnetron sputter deposition of polycrystalline TiN/NbN superlattice coatings. *Surf. Coat. Tech.* **1993**, *57*, 13–18. [[CrossRef](#)]

43. Yashar, P.; Barnett, S.A.; Rechner, J.; Sproul, W.D. Structure and mechanical properties of polycrystalline CrN/TiN superlattices. *J. Vac. Sci. Technol.* **1998**, *A16*, 2913. [[CrossRef](#)]
44. Abadias, G.; Dub, S.; Shmegeera, R. Nanoindentation hardness and structure of ion beam sputtered TiN, W and TiN/W multilayer hard coatings. *Surf. Coat. Tech.* **2006**, *200*, 6538. [[CrossRef](#)]
45. Suszko, T.; Gulbinski, W.; Jagielski, J. The role of surface oxidation in friction processes on molybdenum nitride thin films. *Surf. Coat. Tech.* **2005**, *194*, 319. [[CrossRef](#)]
46. Zhang, X.; Xu, J.; Chai, L.; He, T.; Yu, F.; Wang, P. Carbon and nitrogen co-doping self-assembled MoS₂. *Appl. Surf. Sci.* **2017**, *406*, 30–38. [[CrossRef](#)]



© 2019 by the authors. Licensee MDPI, Basel, Switzerland. This article is an open access article distributed under the terms and conditions of the Creative Commons Attribution (CC BY) license (<http://creativecommons.org/licenses/by/4.0/>).